

# Chapter 9

## Measurements to Support Performance Evaluation of Wireless Communications in Tunnels for Urban Search and Rescue Robots

Kate A. Remley, George Hough, Galen Koepke, and Dennis Camell

**Abstract** We describe general methods for evaluating the over-the-air performance in various radio propagation environments of wireless devices used for control and telemetry of urban search and rescue robots. These methods are based on identification and evaluation of performance metrics that can be used to assess impairments to the wireless link. The type and level of each impairment are derived from measurement data in a given environment, here a subterranean tunnel. We illustrate how parameters can be extracted from the measurement data to determine specific values for the performance metrics and discuss how these values can be used to develop standardized test methods for assessing, verifying, or predicting robot performance.

### 9.1 Performance Requirements for Urban Search and Rescue Robot Communications

Robots have been employed with great success in a wide variety of settings where precise, repetitive, or dangerous tasks need to be carried out. For example, they are commonly found on the production floor of heavy manufacturing facilities where they weld, assemble, and even deliver parts. A relatively new use of robots is in the urban search and rescue (US&R) environment. The majority of robots utilized for potentially dangerous tasks such as explosive ordinance disposal and search and rescue may be considered as extensions of one's eyes, ears, nose, and hands. In this manner, robots have the potential to provide enormous utility for responders that perform vital search and rescue missions at sites of disasters. Robotic sensing devices can access dangerous areas more efficiently in many instances, and can

---

K.A. Remley (✉)

NIST Electromagnetics Division, 325 Broadway, Boulder, CO, USA

e-mail: kate.remley@nist.gov

Work of the United States government, not protected by US copyright.

provide information on trapped or missing people while minimizing the danger to which responders expose themselves at such events.

Wireless telemetry and control of US&R robots is desirable in many situations where, for example, a tether may become tangled, broken, or damaged in debris or other objects in the environment. Evaluation of the performance of the wireless telecommunication devices used for US&R robots typically follows the same fundamental procedures that are used to evaluate wireless devices for civilian applications. Performance evaluation of any wireless device is complicated by the fact that every environment presents a different set of parameters that may impact the wireless device differently. The geometry of features in the environment, the material from which they are made, other radio traffic, and even the movement of the radio within the environment are all factors that may impact the behavior of wireless devices. Evaluating a wireless device in one environment may not adequately represent its performance in another environment. This is not an insurmountable problem. The wireless industry has identified a number of characteristics common to many environments, and from these, they have developed models of representative environments. Devices are designed to perform to a specified level of service within a given type of environment. Wireless device operation is then verified in a test environment whose physical characteristics mimic the representative environment before the device is released for sale. Such "over-the-air" performance evaluation is the focus of this work.

The same general procedure used for civilian devices can be used to predict the performance of wireless communication devices used for US&R robotic applications. For both commercial and US&R applications, the ability to predict performance in real time can also enable real-time modification of system parameters to overcome signal impairments. For example, many wireless devices reduce their transmitted data rate to compensate for a harsh propagation environment. Some robotic systems also may automatically deploy repeaters when signal strength becomes weak. Both of these are examples of intelligent systems.

Because there are some key differences between commercial use of wireless devices and the use of search and rescue robots, existing specifications for wireless device performance are not entirely sufficient for US&R robot applications. Some specifications must either be modified or newly developed. One key difference between the two applications is the need for a high level of reliability in US&R applications. For commercial applications, such as wireless local area networking (WLAN) or cellular telephone communications, if the application is interrupted the user may be inconvenienced, but the session can be reconnected with little more than time lost. Obviously, for US&R use, lives may depend on the reliability of the wireless device, so a higher standard for reliability of service must be applied.

A second difference between many types of commercial wireless applications and US&R robotic applications is that the latter typically involve "point-to-point" radio communications, where the robot and controller interact directly with each other without the use of a base station or other hub that rebroadcasts the signal. Many existing applications, both for commercial wireless and for trunked public safety radio, use the "cellular" model, where a base station serves a number of nodes.

There are some fundamental differences between cellular and point-to-point communication channels. First, for point-to-point communications used in an emergency response event, the transmitter and receiver are often physically closer together than for cellular systems. Second, a cellular base station usually has a much higher elevation than for an emergency response point-to-point scenario. For the robotics application, the robot itself and often the controller, are both located relatively near to the ground, often at a height of one meter or less.

A third difference between commercial wireless applications and US&R applications is that many responder applications involve multiple challenging environmental impairments. For example, cellular telephones are typically designed to operate in outdoor environments, where long delay spreads may result in multipath that can cause intersymbol interference. Emergency response communications often must overcome outdoor multipath as well, but then the responder may enter a large structure, causing significant attenuation in addition to multipath. As another example, many wireless local area networks were designed to operate in home or office environments, where multipath may be overcome by deploying nodes in close proximity to receivers. US&R robots, as well as most emergency response equipment, need to operate reliably within large building structures, in highly reflective industrial environments, and within subterranean tunnels, to name but a few examples. These environments can be much more challenging in terms of reduced received signal level and the amount of both self-interference (multipath) and interference from external sources.

Also, fewer channel models exist for many public-safety environments compared to the well standardized commercial sector. In particular, there is a lack of open-literature data on radio-signal characteristics in responder environments. In the following, we develop methodologies for acquiring and evaluating such data, a key step in development of both performance evaluation metrics and standards for US&R wireless communications.

One final difference between civilian wireless devices and those used by the emergency-response community is the size of the market. Vast resources have been spent on the multi-billion dollar cellular and WLAN communication industries. The public-safety market share is a small fraction of that. The use of wireless technology, other than for voice communications, is relatively new in the emergency-response sector. As a result, few standards exist for specifying the performance of wireless devices for responder applications in responder environments. To mitigate this, the Department of Homeland Security (DHS) Office of Standards is providing resources for development of technically sound performance metrics and standards that cover the use of wireless communications for US&R robots, as well as for other wireless devices used by the response community.

In 2004, the DHS Science and Technology (S&T) Directorate initiated an effort to support the National Institute of Standards and Technology (NIST) in the development of comprehensive standards for testing and certification of effective robotic technologies for US&R applications [1–3]. By assisting in the process of creating such standards, DHS seeks to provide guidance to local, state, and federal homeland security organizations regarding the purchase, deployment, and use of robotic

systems for US&R applications. The NIST/US&R Responder informal advisory board was created, and was able to define over 100 initial performance requirements, and generate 13 deployment categories. The performance requirements were grouped into categories such as human-system interaction, mobility, logistics, sensing, power, and communications. For each requirement, the responders defined how they would measure performance [2].

NIST has since organized a standards effort through ASTM<sup>1</sup> International Standard E54.08 on Homeland Security Standards. In this effort, industry representatives and US&R responders have endeavored to slice the problem into manageable categories. The head of each working group is responsible for producing one or more standard test method that objectively measures a robot's performance in a particular area. Ultimately, the response organization will be able to determine which robots best suit its requirements. Robot researchers and manufacturers will benefit from the definition of test methods and operational criteria, enabling them to provide innovative solutions to meet the universal requirements.

In the area of wireless communications, the performance requirements specified by the responders included:

1. *Expandable Bandwidth*: Will support additional operational components, without loss of data transmission rate, sufficient to allow each component to perform its function.
2. *Range—Beyond Line of Sight*: Must be able to ingress specified number of meters in worst-case collapse. Worst case is a reinforced steel structure.
3. *Security*: System must be shielded from jamming interference and encrypted (to prevent civilians, reporters, and terrorists from listening in).
4. *Range—Line of Sight*
5. *Data Logging—Status and Notes*: Ability to pick up and leave notes.

Items (2) and (4) were designated as critical in the initial standards development effort. Predicting the range of a given robot depends on the technical specifications of the robot's radio link, as well as the radio environment in which the robot is deployed. The technical specifications of the robot's radio are determined by factors such as FCC regulations on output power, frequency of operation, and occupied bandwidth. Additionally, most robot manufacturers rely on the use of existing transmission formats to take advantage of the significant amount of work done on efficient and standardized wireless data transfer by the commercial sector. Consequently, there is little leeway in changing the technical specifications for the radios used in these robots. However, to study the effect of the environment on the range of US&R robots, data needs to be acquired on the radio environments in which robots are likely to be deployed. The Electromagnetics Division at NIST has conducted a multi-year study to acquire open-literature data in several representative environments [4, 5]. After discussing the steps used in evaluating the wireless link

---

<sup>1</sup>Formerly the American Society for Testing and Materials

for US&R robots, this chapter will focus on the methods used for acquiring data to evaluate the expected received-signal characteristics for a given environment. We then discuss how the data can be interpreted to develop models and predict performance of US&R robots in a representative responder environment.

## 9.2 Performance Evaluation Procedures

We describe a commonly used procedure for evaluating the performance of wireless devices and highlight areas where the US&R robot performance evaluation may differ from commercial device evaluation. Procedures are described to identify and extract the key characteristics, or “signal impairments,” that will affect the performance of a wireless device in a given radio propagation environment. Knowledge of these impairments can then be used to classify representative environments for the development of models that can help to predict device performance (such as propagation models or data throughput models), and/or to develop test methods that place the wireless device in a sufficient number of operating states that it can be expected to operate satisfactorily in the field for a given environment. We can summarize this procedure in a few steps:

1. Develop an understanding of how signal impairments impact the performance of a specific wireless device or class of wireless devices.
2. Develop performance metrics that can be used to quantify this impact on performance.
3. Conduct measurements and/or simulations to determine the type and level of signal impairments expected in a given propagation environment.
4. Develop models of, for example, the environment and/or of the system performance, or gather sufficient measurement data in order to predict device performance in the presence of representative impairments.
5. Evaluate device performance when subjected to representative impairments by determining whether the signal impairments cause the device to exceed specified values of performance metrics. This can be done either through measurement verification or, at least for preliminary verification, by looking at the output of the model.

We go through the above procedure step by step. The evaluator first determines what impairments to the received signal affect the performance of the wireless device. Some examples are: a low received signal level, the amount and duration of self or external radio interference, excessive multipath, or the movement of the transmitter relative to the receiver.

Performance metrics are identified that summarize the degradation of device performance when the transmitted signal experiences impairments such as those described above. For example, bit error rate (BER), frame error rate (FER), and block error rate (BLER) are common wireless device performance metrics that indicate a receiver’s inability to accurately decode an impaired signal. For US&R robot

applications, the control channel can easily be evaluated by a go/no-go performance metric. For the video and telemetry links, performance metrics are currently being developed [6, 7].

Based on a representative environment similar to that where the device will be deployed, the evaluator next ascertains what environmental factors create signal impairments, either through measurements or by modeling the environment. Measuring and extracting the type and level of signal impairments in a tunnel environment will be the focus of this chapter. While every tunnel environment will be different, it is possible to identify physical characteristics of tunnels that affect the electrical performance of radio signals. With knowledge of these characteristics, the evaluator can develop or use a model to predict the performance of a robot in other types of tunnel environments.

To benchmark the performance of the wireless device, the evaluator often will set limits on acceptable values for various performance metrics. For example, a performance benchmark for a US&R robot application may be “if the control channel is expected to work 95% of the time in a tunnel environment having  $x$ ,  $y$ , and  $z$  characteristics, the robot is deemed appropriate for use in this type of tunnel environment.” Predictive benchmarking can often be carried out using appropriate models of a given environment. Often, a final measurement verification step is carried out to ensure that the predicted performance approximates the true performance in a representative environment before the models and/or predictions are deemed satisfactory.

An example of this procedure can be illustrated well by the current state-of-the-art in cell phone performance verification. Three key signal impairments that affect the performance of cellular telephones are (a) reduction in received signal level, (b) the existence of multipath (reflected) signals, and (c) the period required for the multipath to decay below a certain amplitude level. For cell phone systems, engineers have developed channel correction algorithms (also called channel equalization) to minimize the effects of (b) as long as the reflections decay within a certain period (c) and the signal attenuation (a) is not beyond the error-correcting capability of the code used.

Cell phone standards bodies have developed propagation channel classifications to describe common environments in terms of the signal impairments (a)–(c). For example, the PB3 model [8] specifies the signal level and amount of multipath likely to be experienced by a pedestrian in an urban environment walking at an average speed of 3 km/h. Extensive data collection has taken place to determine the values of the various signal impairments expected in each of these environments. While not every pedestrian will experience the conditions specified by the PB3 model, standards organizations have determined that this model provides a sufficiently representative description of the signal impairments in these types of environments.

Cell phone system engineers design new cell phones to withstand the signal impairments specified by the PB3 model over a certain percentage of time. In the verification stage, each new model of cell phone that is produced is tested in a facility that simulates the impairments specified by the model. To be accepted for use, the model must meet or exceed the value of the performance metric specified for each relevant application. For example, for a wideband code-division-multiple-

access (W-CDMA) signal, 1.2% BER is specified by the Cellular Telecommunications Industry Association's "over the air" standard.

There are many types of US&R robots being tested for the ASTM standard, including aerial, ground, and aquatic robots. For now the tests target mainly ground robots. Because ground robots move slowly, effects of distortion due to movement (Doppler spread, narrowband fading, and/or wideband fading) are not expected to be an issue. As a result, the main signal impairments expected to degrade the wireless links used by US&R ground robots are also those listed in (a)–(c) above. For applications where the robot goes into or behind a structure, the reduction in received signal strength (a) can be significant. As a second example of the performance evaluation technique described above, we discuss the proposed standardized test method for non-line-of-sight wireless communications. We discuss this test method to illustrate a typical simplified test that captures key performance metrics while providing both portability and repeatability.

The non-line-of-sight test method is intended to simulate the condition where a robot moves behind a building and only a few diffracted signal paths exist between the robot and the operator. The metric that we use for testing the control of the robot is whether the operator can maneuver the robot in a figure-eight pattern. Both measurements and models have been used to develop this test, with the goal of providing a reduction in the signal level comparable to what may be experienced in the field.

In the non-line-of-sight test method, the robot moves 500 m down range from the operator in an open area, such as an airstrip, where reflections are minimal. The robot then turns 90°, moving behind a large obstruction such as a row of large metallic shipping containers stacked two or three high. Once the robot is in a non-line-of-sight condition, the received signal is weak and propagation is ideally limited to a few diffracted paths. The use of a metallic structure enhances repeatability by minimizing the effects of various construction materials, and the use of an open environment enhances repeatability by minimizing multipath reflections. Propagation models of this test environment have helped to optimize the test method in terms of size, shape, and location of the shipping containers for various frequencies of operation and even modulation types. The work presented in the following sections will help with the development of a similarly representative test method for the tunnel environment.

For the tunnel environment discussed below, we will see that once the robot turns a corner in the tunnel, the received signal level drops significantly. The reduction in signal strength is not equal across frequency, however. Received signals at both the lowest and highest frequencies of the test band experience more signal-level reduction than signals at frequencies in the middle of the band.

As we will show, the level (b) and duration (c) of multipath in the tunnel changes, depending on whether or not a line-of-sight path exists. When a line-of-sight exists, the operator may receive the direct-path signal plus one or more strong reflections. The reflected signals can cause deep nulls or sharp increases in the received signal depending on whether the reflections add constructively or destructively with the main signal. Again, we will see that this effect is frequency dependent. Once the

robot has rounded a corner from the operator, all of the received signals arrive via reflected paths. A direct signal plus strong reflections is replaced by multiple weaker reflections and the received signal takes on a much noisier appearance.

Well-developed channel propagation models exist for tunnel environments. Thus, for many wireless applications, including the US&R robot application, it is possible to extract the level of signal impairment in one tunnel and derive the expected level of impairment for another tunnel. The key to using this predictive method of performance evaluation effectively is extraction of signal impairments that are expected for the application at hand. In our case, data must be gathered under conditions that represent the US&R robot operating conditions mentioned in the introduction, including point-to-point communications and low-to-the-ground operation. We will demonstrate a method for acquisition and extraction of data and its use in models that predict the performance of one type of US&R robot. We can verify the model by measuring the performance of the robot under the same conditions as those where the model parameters were extracted. We then describe how this model can be used to predict the performance of robots in a tunnel more representative of the type encountered in US&R operations. Throughout, the goal of the work is to present a framework for performance evaluation, rather than to conduct a comprehensive evaluation of a specific robot in a specific environment.

### **9.3 Measurement of Signal Impairments in a Tunnel Environment**

Researchers from the Electromagnetics Division of the National Institute of Standards and Technology and the Fire Department of New York (FDNY) conducted field tests to quantify the expected type and level of signal impairments in a representative tunnel environment. Tests were conducted at the Black Diamond Mines Regional Park near Antioch, California on March 19–21, 2007. The goal of these field tests was to investigate propagation channel characteristics that affect the reliability of wireless telemetry and control of US&R robots in tunnels and other weak-signal environments. In this section, we describe measurement methods used to study parameters relevant to robot performance.

We used both time- and frequency-domain techniques to study the signal attenuation (loss) and reflections (multipath) that may impair successful wireless communications in tunnels. We also directly evaluated the performance of both the video and control links for a robot inside one of the mine tunnels. In this section, we summarize the data we collected and interpret the key findings from the study, which is described in its entirety in [5]. In the next section, we use the measured data to model both path loss and channel capacity in tunnels. The models are verified by comparison to our tests of the robot in the tunnel. Models such as these can be used to predict robot performance in tunnels having characteristics different from the ones we measured, such as subways and utility tunnels, as shown in Section 9.5.

Recently, the wireless field has seen a renewed interest in studies of signal propagation in both mine and subway tunnels, following a good deal of study on mine communications in the 1970s. A seminal work on mine tunnel propagation by Emslie et al. [9], studied radio wave propagation in small underground coal tunnels (4.3 m wide  $\times$  2.1 m high) for frequencies ranging from 200 MHz to 4 GHz. Emslie's model for propagation in tunnels is still used today. Recently, Rak and Pechak [10] applied Emslie's work to small cave galleries for speleological applications, confirming Emslie's findings that once a few wavelengths separate the transmitter and receiver, the tunnel acts as a waveguide that strongly attenuates signals below the waveguide's cutoff frequency. Because the walls of the tunnel are not perfectly conducting, signals operating above the cut-off frequency also experience significant loss. In a recent paper, Dudley et al. [11] performed a detailed assessment of operating frequency in a variety of tunnels. They found that as frequency increases, the lossy waveguide effect decreases.

Other work on propagation measurement and modeling in mine tunnels was reported in [12], whose group conducted narrowband and wideband measurements centered at 2.4 GHz. A model that describes tunnel propagation as a cascade of impedances was reported in [13, 14]. Studies of radio wave propagation in subway tunnels at 945 MHz and 1.853.4 GHz were presented in [15]. A ray tracing model was implemented to study the effects of the tunnel geometry and materials on propagation.

Our measurements, covering a much wider frequency range than [11–15], and implementation of the model of [10] confirm the lossy waveguide effect in the tunnels we studied. This effect can have a significant impact on the choice of frequency for critical applications such as US&R operations, where typically infrastructure such as a repeater network is not available and lives may be at stake.

Another factor in tunnel communications is multipath caused by reflections off the walls, floor, and ceiling of the tunnel. This was clearly seen in the work of Dudley, et al. [11] and was studied carefully over a 200 MHz bandwidth in [12]. Multipath can have a pronounced effect on successful transmission of wideband data. Some types of multipath interference may affect certain frequencies in a wideband signal while simultaneously having little impact on other frequencies. This frequency selectivity can make decoding signals difficult for the demodulator in a receiver.

We studied the frequency selectivity of the multipath in the tunnel environment by measuring the received signal power across a wide frequency range. We studied the decay time of the multipath by measuring the root-mean-square (RMS) delay spread, a common figure of merit that describes the period needed for reflected signals to decay below a threshold value. We compare our measured results to a model of channel capacity based on a modified form of Shannon's theory of channel capacity [16]. This theorem provides a basis for predicting the success of wireless communication in multipath environments.

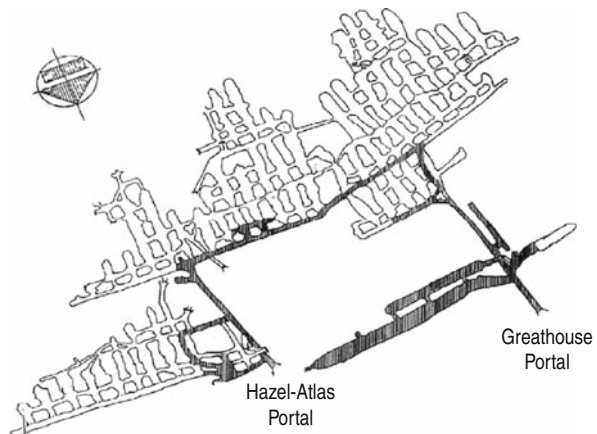
We will first describe the tunnel environment where we made the measurements. We next discuss the types of measurements we made in sufficient detail so that other organizations could reproduce them in other environments. We give selected results

of the measurements and a brief interpretation of the results. Finally, we report on tests made of the control and video channels of a robot in this tunnel environment.

### 9.3.1 The Test Environment

The Black Diamond Mines are part of an old silica mine complex that was used early in the 1900s to extract pure silica sand for glass production. As such, the walls of the mine shafts are rough and consist of sandy material. Two tunnels were studied, the Hazel-Atlas North (here called the “Hazel-Atlas” tunnel) and Hazel-Atlas South (here called the “Greathouse” tunnel). The tunnels are located beneath a mountain and are joined together several hundred meters inside, as shown in Fig. 9.1. Several chambers and tunnels intersect with the main tunnels, some of which reach the surface to provide air shafts. These airshafts can create alternative paths for RF signals traveling within the mine complex.

**Fig. 9.1** Overview of the Black Diamond mine tunnel complex. The *dark-shaded* areas are accessible. The distance between the two portals is around 400 m.



The cross-sectional dimensions of the Hazel-Atlas tunnel varied from approximately 1.9 m (6', 3'')  $\times$  1.9 m to as much as 2.6 m (8', 5'')  $\times$  2.4 m (8', 0''). The dimensions of the Greathouse tunnel were somewhat bigger, up to approximately 3 m square in places. The Hazel-Atlas tunnel contained railroad tracks spaced 61 cm (24'') apart. Both tunnels consisted of a straight section followed by a 90° turn around a corner, as shown in Fig. 9.1.

Figure 9.2 shows photographs of the Hazel-Atlas tunnel. Figure 9.2(a) shows the portal (entrance) of the Hazel-Atlas mine and Fig. 9.2(b) shows a location deep inside the tunnel. The photographs show the rough, uneven walls in the tunnels, some with wooden shoring, and railroad tracks. Figure 9.3 shows photographs of the Greathouse tunnel. Figure 9.3(a) shows the receive antenna located at the junction of the large chamber where it meets the Greathouse tunnel just inside and to the left of the portal. This was our reference location. Figure 9.3(b) shows a wooden walkway deep inside the Greathouse tunnel.



**Fig. 9.2** (a) Portal into the Hazel-Atlas mine tunnel. (b) Wood shoring approximately 150 m into the tunnel. The robot tested can be seen on the cart between the railroad tracks



**Fig. 9.3** (a) Receive antenna site in the Greathouse mine tunnel. (b) Walkway at the top of the stairs in the Greathouse tunnel

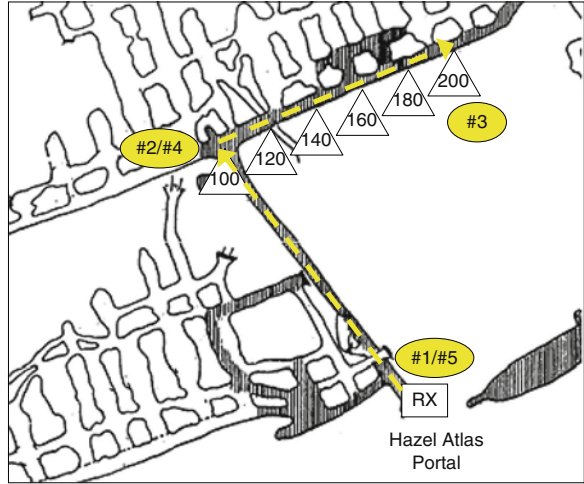
### 9.3.2 Measurements

#### 9.3.2.1 Narrowband Received Power

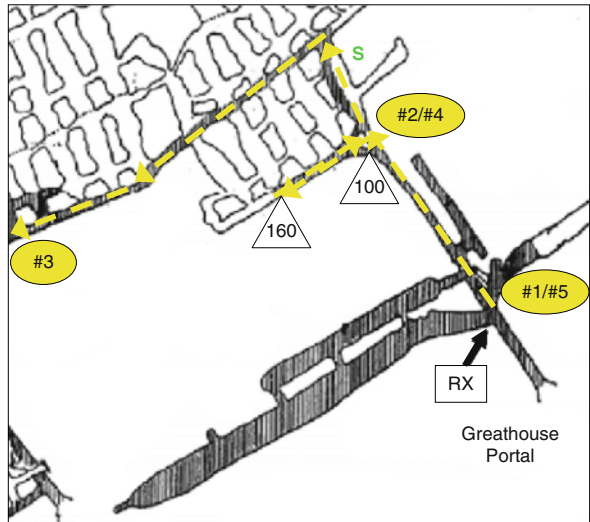
We measured the received power from a transmitter placed at various locations inside the tunnels. We collected single-frequency (unmodulated) received-power data at frequencies near public-safety bands (approximately 50, 160, and 450 MHz). Gathering information at these frequencies helps to provide a choice of optimal frequency for the US&R community for this environment, both for robot communications and for other types of radio communication. These data provide insight into the lossy waveguide effect mentioned in the Introduction.

The handheld transmitters used were radios similar to those of first responders, except they were placed in ruggedized cases and were modified to transmit continuously. Each radio transmitted a signal of approximately 1 watt through an omnidirectional “rubber duck” antenna mounted on the case. During the tests, the radio antennas were approximately 0.75 m from the floor, a height similar to that of the robot we studied.

We carried the radio transmitters from the receive antenna location to locations deep within the tunnels while continuously recording the received signal. From the Hazel-Atlas tunnel portal, we carried the transmitter approximately 100 m down a straight tunnel, then turned a corner and proceeded another 100 m, as shown in Fig. 9.4(a). For the Greathouse tunnel, we went deeper into the mountain, as shown in Fig. 9.4(b). We carried the transmitter approximately 100 m down the tunnel, turned left and took an approximately 60 m hairpin path in order to continue



(a)



(b)

**Fig. 9.4** (a) Close-up view of the Hazel-Atlas tunnel. (b) Close-up view of the Greathouse tunnel. The dashed lines show the paths along which we took measurements, including the 90° turns at 100 m in both tunnels. The triangles indicate the distance in meters, the ovals correspond to locations shown in Figs. 9.5 and 9.6, and the receiving equipment is labeled RX

further into the tunnel. After the hairpin, we climbed several stairs (marked “S” in Fig. 9.4(b)), turned left and continued approximately 120 m almost to the junction with the Hazel-Atlas tunnel. We then returned by the same route.

The receiving equipment was located just outside the portal for the Hazel-Atlas measurements, and at the junction of the Greathouse chamber and the main tunnel for the Greathouse measurements. Omnidirectional disccone receiving antennas were mounted on tripods, as shown in Fig. 9.2(a). We used a narrowband communications receiver to convert the received signal to audio frequencies, where it was digitized by a computer sound card and recorded on a computer. This instrument, when combined with NIST-developed post-processing techniques [5, 17], provides a high-dynamic-range measurement system that is affordable for most public-safety organizations. Part of the intent of this project was to demonstrate a user-friendly system that could be utilized by US&R organizations to assess their own unique propagation environments. A rough estimate for the uncertainty in this measurement, based on repeat measurements, is on the order of 1 dB [17]. The variability in received power due to antenna placement within the environment is on the order of 10 dB, much higher than the expected uncertainty. As a result, we do not report measurement uncertainties on our graphs.

Figures 9.5 and 9.6 show measured received-power data at frequencies of 50, 162, and 448 MHz acquired while the transmitters were carried by foot through the Hazel-Atlas and Greathouse tunnels, respectively. The signals were sampled at approximately 48 kHz and the power averaged over 1-second intervals. The left and right halves of the graph show measurements made walking into and out of the tunnels, respectively, and thus mirror each other. The vertical dashed lines on the graph correspond to the entrance (#1, #5), turn (#2, #4), and turn-around point (#3), as shown in Fig. 9.4(a) and (b).

In Fig. 9.5, the small increases in received power shown as bumps between points 2–3 and 3–4 in the Hazel-Atlas tunnel illustrate an alternative signal path through one of the air vents located in the small chambers off the main tunnel. The size of the air vent relative to the wavelength determines how significant this additional path is. The small increases in received signal power in the Greathouse tunnel, shown between points 2–3 and 3–4 in Fig. 9.6, are caused by an additional signal path encountered at the junction of the main tunnel and the stairwell 100 m into the tunnel (denoted by an “S” in Fig. 9.4(b)). This additional signal path was encountered after the hairpin, as the transmitter returned to the junction labeled #2/#4 in Fig. 9.4(b). The horizontal lines in the graphs indicate that the received signal levels are below the noise floor of the receiver; that is, less than approximately  $-130$  dBm.

We see from both Figs. 9.5 and 9.6 that the lower frequencies drop off more rapidly as the transmitter moves deeper in the tunnel within the first 100 m of the test (between points 1–2 and 4–5). This rapid attenuation is due to the lossy waveguide effect described in references [5, 9–11]. The signals for the 448 MHz carrier frequency (Figs. 9.5(c) and 9.6(c)) exhibit less attenuation, and this is where the models of [9] may apply. Signals may travel even further at higher frequencies, as discussed in [9–11]. This frequency dependence may play a significant role in

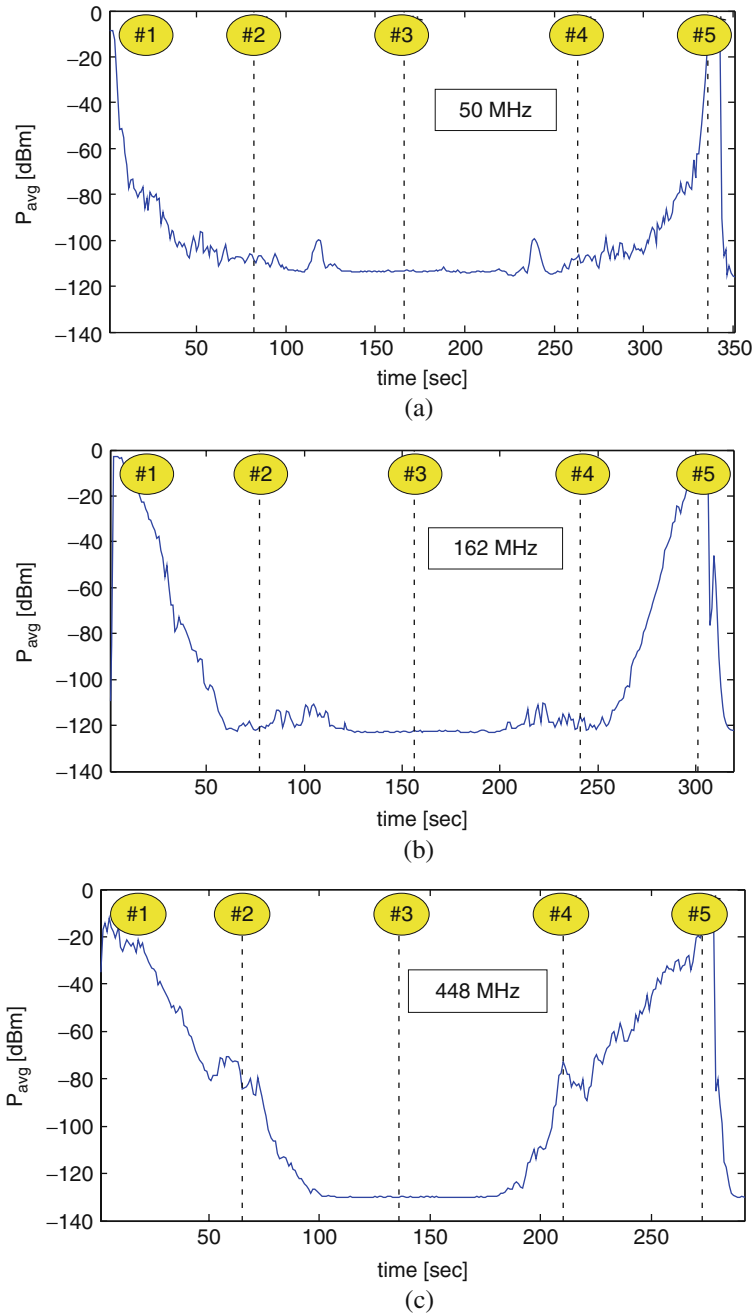


**Fig. 9.5** Received-power data in the Hazel-Atlas Mine for three carrier frequencies: (a) 50 MHz, (b) 162 MHz, (c) 448 MHz. In each case the #2 and #4 vertical *dashed lines* correspond to the turn at 100 m: once on the way into the tunnel and once on the way out. The #3 *dashed line* represents the end point. For the Hazel-Atlas mine tunnel, the end was at 200 m, shown in Fig. 9.4(a)

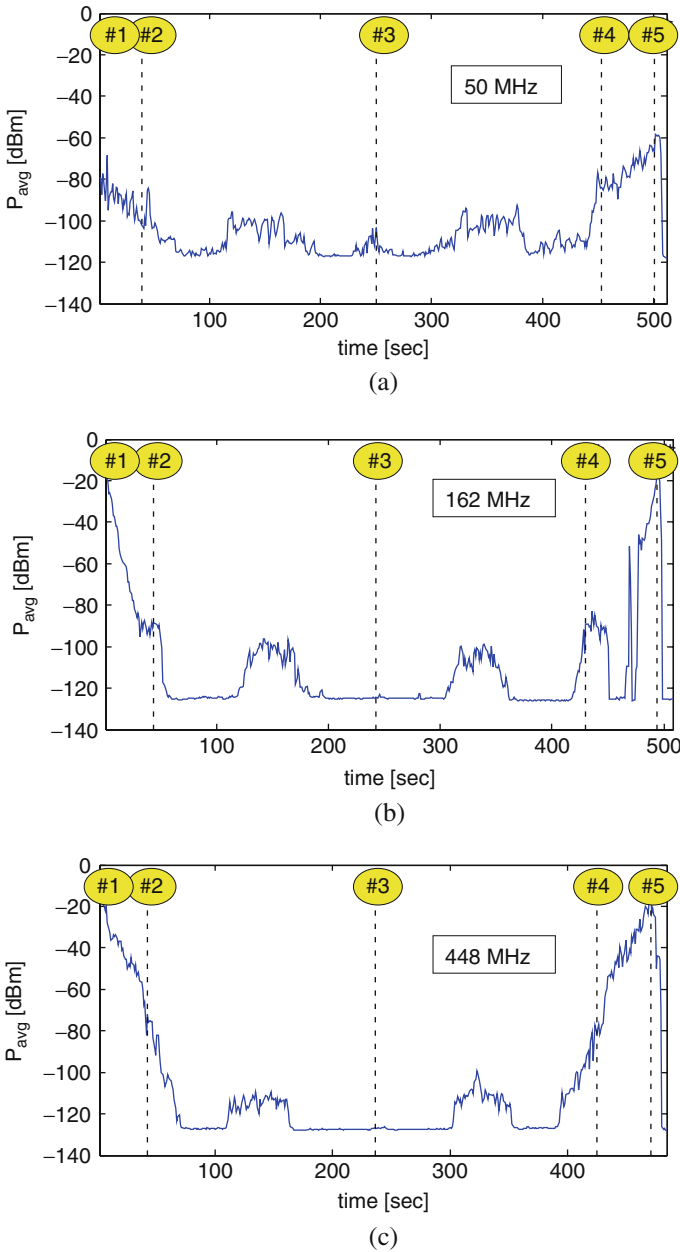


**Fig. 9.6** Received-power data in the Greathouse Mine tunnel for three carrier frequencies: (a) 50 MHz, (b) 162 MHz, (c) 448 MHz. In each case the #2 and #4 vertical dashed lines correspond to the turn at 100 m: once on the way into the tunnel and once on the way out. The #3 dashed line represents the end point. For the Greathouse mine tunnel, the end point was approximately 350 m into the tunnel, as shown in Fig. 9.4(b)

deciding which frequencies to utilize in US&R robot deployment applications, as will be discussed in Section 9.4.

The exact waveguide cut-off frequency for this type of tunnel is difficult to define, because the walls behave as lossy dielectrics rather than conductors. These conditions are discussed in [18], where the attenuation constant is found to vary as the inverse of frequency squared (Section 2.7, pp. 80–83). Hence, we would expect higher attenuation at the lower frequencies but no sharp cut-off. Further complications in the Hazel-Atlas tunnel are the axial conductors (cables, water pipes, rails) that may support a coaxial-cable-like mode of propagation, the irregular cross-section, and the side chambers and tunnels.

### 9.3.2.2 Excess Path Loss and RMS Delay Spread

We also conducted measurements at several stationary positions within the tunnels covering a very wide frequency band. These “excess-path-loss” measurements provide the received signal power relative to the theoretical direct-path loss in free-space as a function of frequency. Excess path loss is a metric that describes signal impairments in a propagation channel over and above simple signal reduction due to distance. Excess path loss can help to characterize the multipath in a given channel: At each measured frequency, we retain the phase relationships between the transmitted and received signals, enabling reconstruction of time characteristics of the signal through the Fourier Transform. In the absence of reflections, the measured wide frequency band yields a short-duration pulse. In a multipath environment, the period needed for the reflected copies of the pulse to decay can be used to study the number and duration of multipath reflections in an environment.

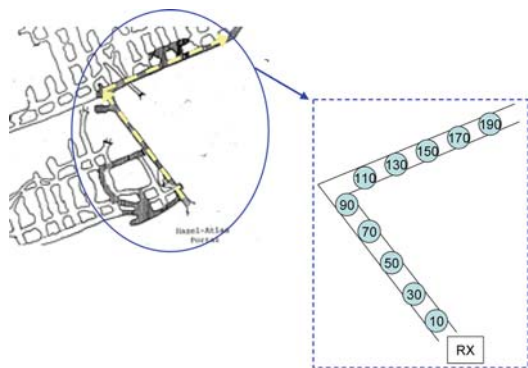
Our “synthetic-pulse,” wideband-frequency-measurement system is based on a vector network analyzer (VNA). Our measurements covered frequencies from 25 MHz to 18 GHz. The post-processing and calibration routines associated with it were developed at NIST [19]. In the synthetic-pulse system, the VNA acts as both transmitter and receiver. The transmitting section of the VNA sweeps over a wide range of frequencies a single frequency at a time. The transmitted signal is amplified and fed to a transmitting antenna. For this study, we used omnidirectional disccone antennas for frequencies between 25 MHz and 1.6 GHz, and directional horn-type transmitting and receiving antennas for frequencies between 1 GHz and 18 GHz. We used directional antennas to provide additional gain in the direction of propagation, because the signals received from deep within the tunnels were quite weak. While some US&R robot manufacturers use directional antennas in weak-signal conditions, many use omnidirectional antennas exclusively. Note that if omnidirectional antennas were used in the higher frequency band, certain channel parameters, including the RMS delay spread, would have somewhat different values than those measured here.

The received signal was picked up over the air in the tunnel by the receiving antenna and was relayed back to the VNA via a fiber-optic cable. The fiber-optic cable maintains the phase relationships between the transmitted and received signals, enabling post-processing reconstruction of time-domain effects associated

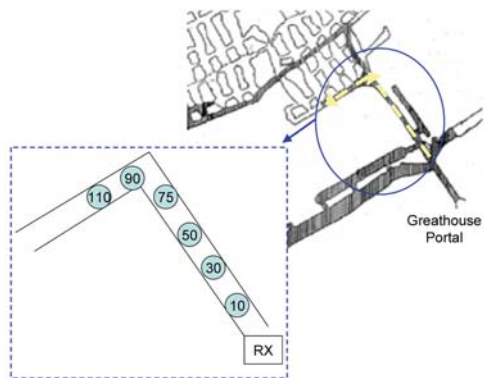
with the received signal such as the power-delay profile. The broad range of frequencies and time-domain representation provide insight into the reflective multipath nature of the tunnel that cannot be captured by use of single-frequency measurements. The receiving antenna must remain fixed during each measurement, so these tests are carried out at discrete locations, unlike the single-frequency tests.

We measured excess path loss every 20 m starting approximately 10 m from the transmitting antenna, as shown in Fig. 9.7(a) and (b). The VNA was located at the Hazel-Atlas portal (Fig. 9.7(a)) and in the Greathouse chamber (Fig. 9.7(b)). The transmitting antenna was located at the portal for the Hazel-Atlas tunnel and at the junction of the chamber and the tunnel for the Greathouse tunnel.

Figure 9.8(a)–(c) show measured excess path loss over a frequency band from 25 MHz and 1.6 GHz for increasing distances into the Hazel-Atlas tunnel. These graphs are all at distances less than 100 m; that is, before the right-angle turn. The top curve in each graph represents the received power level, referenced to the



(a)



(b)

**Fig. 9.7** Data-collection locations for the synthetic-pulse measurements.  
(a) Hazel-Atlas mine tunnel.  
(b) Greathouse mine tunnel

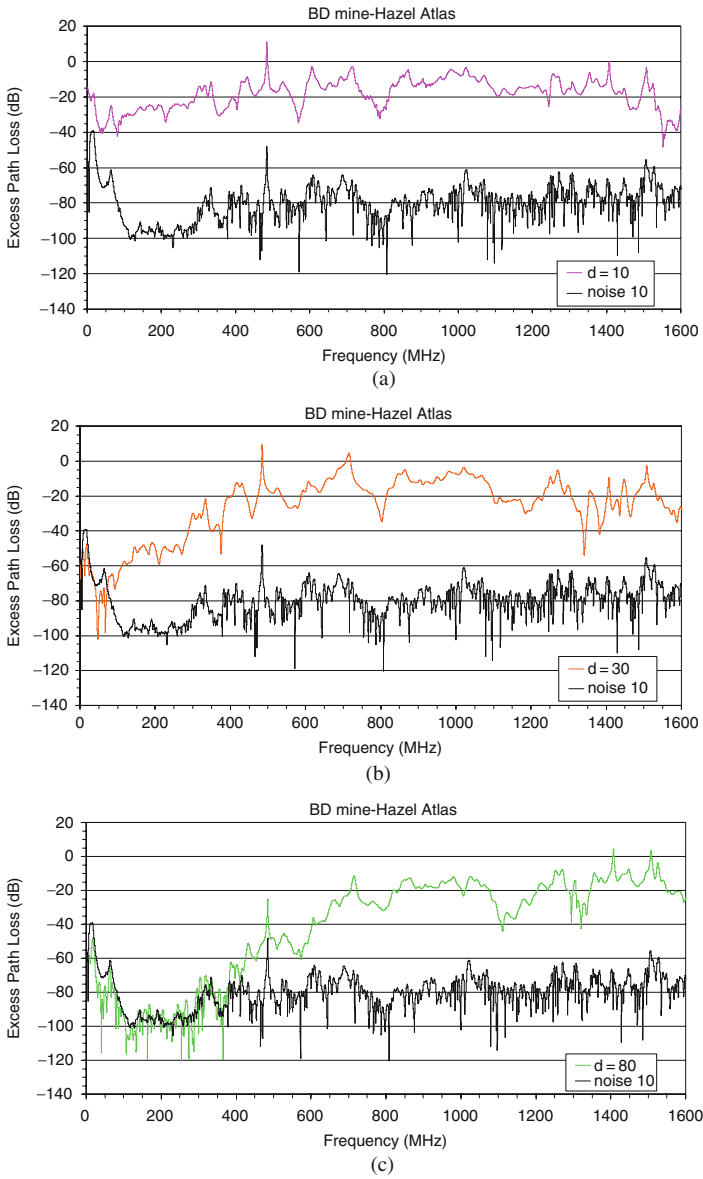


**Fig. 9.8** Excess path loss measurements from 25 MHz to 1.6 GHz carried out at different distances: (a) 10 m, (b) 30 m, and (c) 80 m from the portal of the Hazel-Atlas mine tunnel. The “noise” curves were measurements taken with no transmitted signal. These were not made at every location, and are presented to give an indication of the dynamic range of each measurement (received signal power relative to noise power)

calculated free-space path loss at that location. The bottom curve represents the noise floor of the measurement system, to provide an indication of the dynamic range of each measurement.

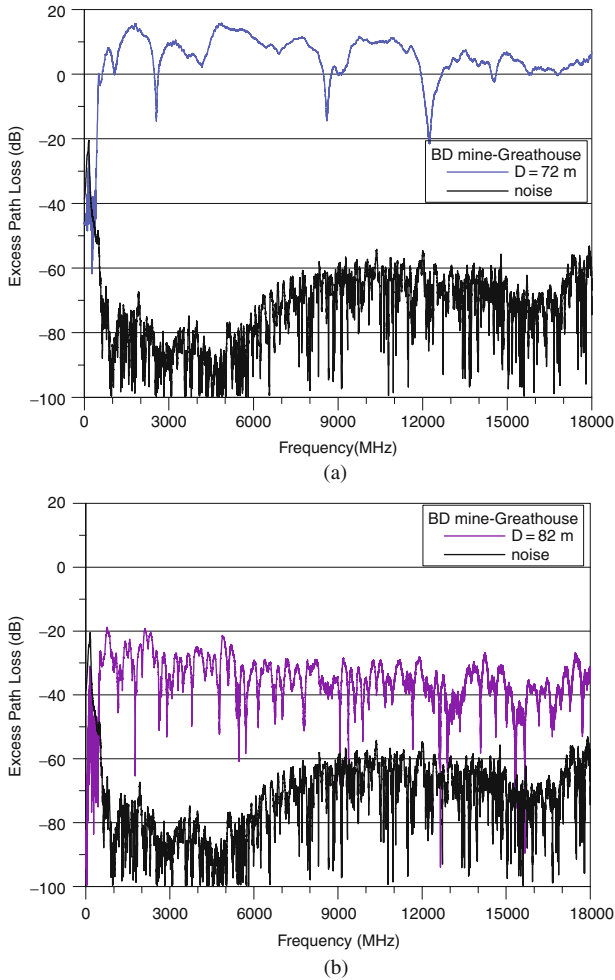
The graphs of Fig. 9.8 show data starting from 0 Hz; however, the valid (calibrated) measurement range is stated for each graph. A rough estimate for the uncertainty in this measurement based on the VNA manufacturer's specifications is on the order of 0.2 dB. The variability in received power due to antenna placement within the environment is on the order of 10 dB, higher than the expected uncertainty. Thus, we do not report measurement uncertainties on our graphs.

Figure 9.8 shows that in a line-of-sight condition, the spectrum of the received signal displays significant frequency dependence. At frequencies between 25 MHz and 1.6 GHz, the lossy waveguide effect is shown by the rapidly decreasing signal on the left-hand side of the graph. We see that a carrier frequency higher than approximately 700 MHz would suffer less loss compared to lower frequencies in this particular tunnel. The same type of low-frequency attenuation was seen in the Greathouse tunnel as well.

Figure 9.9(a) and (b) show the excess path loss for frequencies from 1 GHz to 18 GHz in the Greathouse tunnel. Again, this is the path loss or gain that would exceed the free-space path loss at each location. For this measurement, the transmitter was located within the tunnel itself and, unlike for the Hazel-Atlas tunnel shown in Fig. 9.8, the reflections from the tunnel actually increase the power at the location of the receiver for some frequencies, shown by the excess path loss greater than 0 dB.

Figure 9.9(a) shows well defined nulls and peaks, corresponding to a direct path plus one or more strong reflections, when a line-of-sight path exists. This is characteristic of a "Rician" fading profile. Figure 9.9(b) shows that once the receiving antenna turns the corner, the signal takes on a more random variation with frequency, because transmission consists of only reflected signals. This is characteristic of a "Rayleigh" fading profile. We see that the average received signal level is relatively constant with frequency, but the peaks and nulls are significant.

Finally, we present the RMS delay spread for the two mine tunnels in Table 9.1 for frequencies from 25 MHz to 1.6 GHz and 1 to 18 GHz. An error analysis for these data is in process; consequently, we report no uncertainties in the RMS delay spread. We see that the shortest delay spreads are found by use of the directional antennas, as expected since reflected signals arriving from directions located behind the receive antenna are not received. A comparison of the effect on the RMS delay spread of using omnidirectional versus directional receive antennas in high multipath environments can be found in [20]. The delay spread in the line-of-sight case is nearly the same as for the non-line-of-sight case because of the strong multipath in the line-of-sight condition. In many environments, the line-of-sight delay spread is shorter because of a strong direct-path signal. The complete set of excess-path-loss data is given in [5].



**Fig. 9.9** Excess path loss for frequencies from 1 to 18 GHz in the Greathouse tunnel (a) 72 m into the tunnel in a line-of-sight condition, and (b) 82 m into the tunnel in a non-line-of-sight condition

### 9.3.2.3 Tests of Robot Communications

We also carried out tests on a commercially available robot in the Hazel-Atlas tunnel. Control and video were as-built for the commercial product. We used the omnidirectional antennas that came with the system for all tests in order to assess the default capabilities of this robot. The robot we used is controlled with a spread-spectrum, frequency-hopping protocol, which was configured to transmit in the unlicensed 2.4 GHz industrial, scientific, and medical (ISM) band. The control channel utilizes a modulation bandwidth of approximately 20 MHz. The output power of the bidirectional control link is nominally 500 mW.

**Table 9.1** RMS delay spread for the Hazel-Atlas and Greathouse mine tunnels

Distance (m)	Hazel Atlas tunnel		Greathouse tunnel	
	Low frequencies (ns)	High frequencies (ns)	Low frequencies (ns)	High frequencies (ns)
0	31.0	14.4	–	–
10	25.3	17.6	22.7	3.2
20	18.5	7.6	14.3	5.0
30	15.9	15.0	15.2	3.8
40	17.0	11.5	17.6	4.0
50	15.5	13.1	21	19.3
60	19.7	20.6	18.1	7.3
70	17.2	11.1	23.1	11.6
80	15.2	10.0	14.2	3.8
90	15.2	8.4	–	–
100	15.7	9.6	10.0	3.7
110	x	7.5	19.8	4.1

Left columns: Frequencies from 25 MHz to 1.6 GHz measured with omnidirectional antennas. Right columns: Frequencies from 1 to 18 GHz measured with directional antennas. The gray-shaded areas represent a non-line-of-sight propagation condition. The “x” at 110 m in the Hazel-Atlas tunnel indicates that the received signal was too weak to calculate the RMS delay spread

The robot transmits video by use of one of ten channels between 1.7 and 1.835 GHz. The robot we tested transmitted at 1.78 GHz by use of an analog modulation format that was non-bursted and non-frequency-agile. The video channel utilized approximately 6 MHz of modulation bandwidth. The output power was nominally 2 W.

The robot controller was located at the entrance to the tunnel, shown in Fig. 9.10. We positioned the robot inside the tunnel after the first bend in a non-line-of-site condition. The robot was moved through the tunnel on a cart, shown in Fig. 9.2(b), so that we could check the control link even after video was lost. Every 10 m, the video quality and control link were checked. Video was rated qualitatively by the



**Fig. 9.10** (a) Robot operator positioned at the entrance to the Hazel-Atlas mine tunnel. (b) The robot was operated in a non-line-of-sight condition more than 100 m inside the tunnel

robot operator, and control was checked by the ability of the operator to move the robot arm, and verified by a researcher in the tunnel. No attempt was made to provide more granularity in these tests; that is, we assumed that moving the arm up was equivalent to moving it down or rotating it.

Table 9.2 shows the results of our tests. We were able to communicate with the robot in a non-line-of-sight condition deep within the tunnel. This is consistent with the results of Figs. 9.8 and 9.9, which indicate that signals in the low gigahertz range should propagate farther than those at lower frequencies.

**Table 9.2** Results of robot wireless communication link tests carried out inside the Hazel-Atlas tunnel at Black Diamond Mines Regional Park

Distance in tunnel (m)	Video quality (1.7 GHz)	Control of arm (2.4 GHz)
100	good	yes
110	good	yes
120	poor (intermittent)	yes
130	poor (intermittent)	yes
140	very poor	yes
150	none	yes
160	none	delay experienced
170	none	intermittent control
180	none	delay experienced
190	none	delay experienced
200	none	delay experienced
205	none	none

Table 9.2 also shows that control of the robot was possible much deeper into the tunnel than where we were able to receive video, even though the output power of the video channel was higher (2 W for video vs. 0.5 W for control). A much higher data rate is necessary to maintain high-quality video transmission, as opposed to the relatively small amount of data needed to control the robot. Transmitting this large amount of data requires a higher received signal strength than for the control channel; therefore, failure of the video before the control is not unexpected. The delay experienced in controlling the robot when it was deep in the mine indicates packet loss and resend for error correction under weak-signal conditions.

## 9.4 Modeled Results

### 9.4.1 Single-Frequency Path Gain Models

To study the extent of signal attenuation and waveguiding in these tunnels, we implemented an analytical model that simulates signal propagation in tunnel environments having various physical parameters [9, 10, 21]. Briefly, the model assumes

a single dominant mode in a lossy rectangular waveguide with the attenuation  $\alpha$  in dB/m expressed for vertical polarization as

$$\alpha = \alpha_{\text{TUNNEL}} + \alpha_{\text{ROUGHNESS}} + \alpha_{\text{TILT}}, \tag{9.1}$$

where

$$\alpha_{\text{TUNNEL}} = 4.343\lambda^2 \left( \frac{1}{a^3\sqrt{\epsilon_R - 1}} + \frac{\epsilon_R}{b^3\sqrt{\epsilon_R - 1}} \right), \tag{9.2a}$$

$$\alpha_{\text{ROUGHNESS}} = 4.343\pi^2 h^2\lambda \left( \frac{1}{a^4} + \frac{1}{b^4} \right), \tag{9.2b}$$

$$\alpha_{\text{TILT}} = 4.343 \frac{\pi^2\theta^2}{\lambda}, \tag{9.2c}$$

$\lambda$  is the wavelength,  $a$  is the width of the tunnel,  $b$  is the height of the tunnel, and  $h$  is the roughness, all in meters. Other parameters include  $\epsilon_R$ , the dielectric constant of the rock walls, and  $\theta$  is the angle of the tunnel-floor tilt in degrees.

We set the parameters of the model to approximate the Hazel-Atlas tunnel, given below in Table 9.3. This model works well only for frequencies well above the cut-off frequency; that is, for wavelengths significantly less than the dimensions of the tunnel [9, 10]. Hence, in Fig. 9.11 we compare measured and modeled results for only 448 MHz.

**Table 9.3** Parameters used in the tunnel model

Parameter	Value
Width	2 m
Height	2 m
Wall roughness	0.3 m
$\epsilon_R$	6
Tilt	1°

In Fig. 9.11, the increase in measured signal strength at a distance of around 80 m, is caused by signal propagation through an air vent as well as through the tunnel, as was seen in Fig. 9.5. The agreement between the measured and modeled data led us to conclude that waveguiding plays a significant role in radio propagation in these tunnels.

The model also lets us explore which frequencies may be optimal for robot or other wireless communications in the tunnel. Figure 9.12 compares a number of commonly used emergency responder frequencies as a function of distance within the tunnel.

As discussed in [9, 10], the frequency-dependent behavior of the tunnel leads to a “sweet spot” in frequency. Below the sweet spot, signals do not propagate well, due to the effect of waveguide-below-cutoff attenuation and wall loss. Above the sweet spot, free-space path loss (which increases with frequency) and  $\alpha_{\text{TILT}}$  dominate, and signals do not propagate well. Again, models such as these may enable a choice

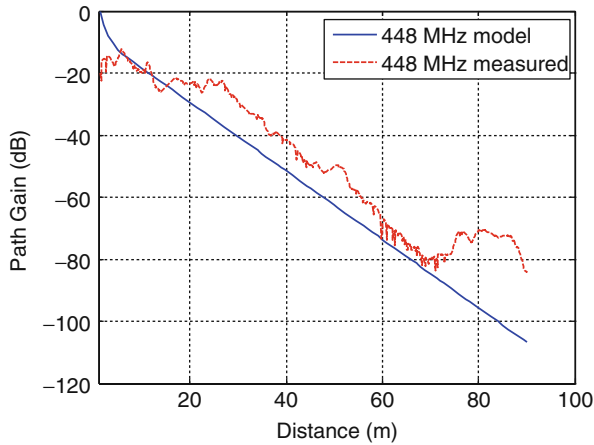


**Fig. 9.11** Comparison of measured and modeled data for the Hazel-Atlas tunnel. The carrier frequency is 448 MHz. The modeled data simulate waveguide propagation for a waveguide whose physical parameters approximate those of the tunnels

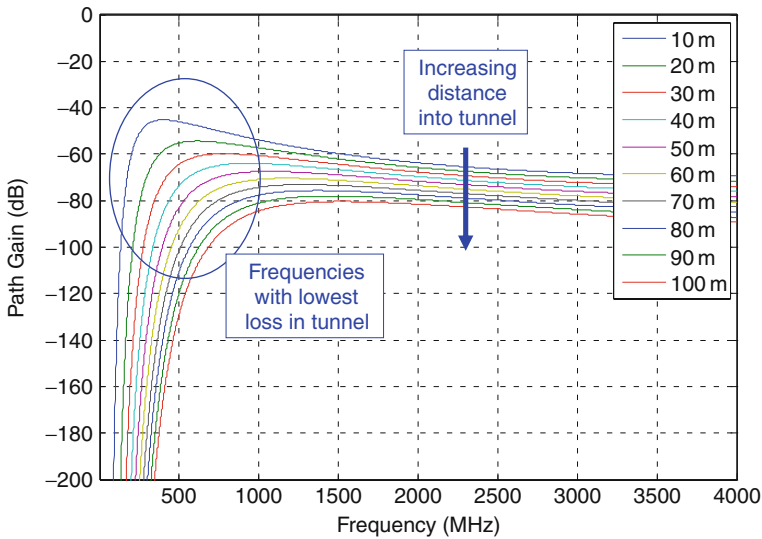
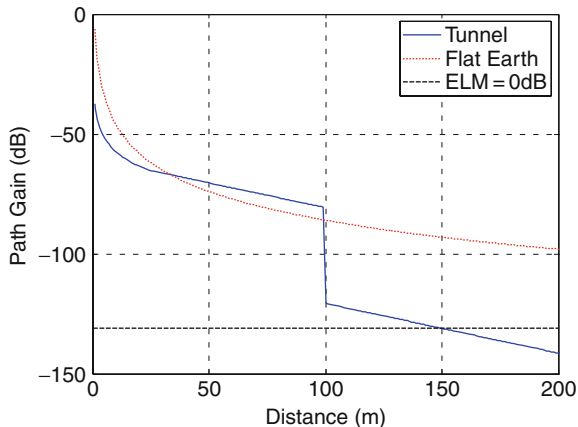


**Fig. 9.12** Path gain versus frequency for various distances in a tunnel having physical characteristics similar to those of the Hazel-Atlas tunnel. Frequencies of approximately 400 MHz–1 GHz propagate further than either lower or higher carrier frequencies

of appropriate frequency for US&R robot communications in tunnel environments. Note that these results are valid only for a tunnel with these dimensions, wall materials, and surface roughness. The curves would need to be recalculated for other types of tunnels.

We also used the model to investigate the video performance of the robot, described in Section 9.3.2. The frequency-hopping control channel would need to be

**Fig. 9.13** Path gain curves for a tunnel with a right-angle turn at 100 m (solid) and the flat earth (dotted) environment. The curve labeled “ELM = 0 dB” indicates where the excess link margin calculation predicts loss of signal. As shown, this occurs approximately 150 m into the tunnel



modeled by use of other methods, because it consists of several narrowband channels that frequency hop within a wide modulation bandwidth. In Fig. 9.13, we plot the estimated path gain at a carrier frequency of 1.78 GHz for the tunnel environment with a right-angle turn 100 m from the receiver. We used the parameters in Table 9.3 for the model. A path gain of  $-40$  dB was used as an approximation for the turn in the tunnel at 100 m, based on work done by Lee and Bertoni in [22]. We plot the flat-earth path gain for comparison. The flat-earth model [23] is commonly used to represent line-of-sight propagation in a low-multipath, outdoor environment. In this model, signals propagate between the transmit and receive antennas along two paths only: a direct path and a single reflection off of the ground. This is in contrast to the high-multipath, waveguiding channel encountered in the tunnel.

Figure 9.13 also shows the theoretically computed excess link margin (ELM). The ELM is the difference between the received signal strength and the minimum receiver sensitivity. The receiver sensitivity is determined by the thermal noise of the receiver and the receiver’s front-end amplifier noise (5 dB, as a rule of thumb). The thermal noise is given by  $N = kTB$ , where  $k$  is the Boltzmann constant,  $T$  is the temperature in kelvins, and  $B$  is the bandwidth of the receiver. In order for a wireless link to be maintained, the ELM usually must be greater than zero dB.

The ELM plotted in Fig. 9.13 agrees well with the measured results from Table 9.2, which show that the video completely drops out between approximately 140 and 150 m. Given the fluctuation in signal strength due to multipath in this tunnel environment, once the link margin drops below 10 dB at approximately 120 m, the video quality degrades and the picture becomes intermittent.

### 9.4.2 Channel Capacity Model

In general, received RF power and modulation bandwidth effectively place an upper bound on the capacity of a communications link. That is, a link exists between the capacity, bandwidth, and signal-to-noise ratio in any propagation environment. The

Shannon channel capacity theorem [16] helps to explain how these factors affect the useful distance over which a robot can return a wideband signal such as a video image or control signal. For example, in order to compare robot X that uses four cameras with robot Y that uses two cameras, the user should understand that if both robots use the same transmission bandwidth, robot Y should transmit video further than robot X.

The channel capacity estimate provided by the Shannon theorem will be crude for a tunnel environment because the Shannon theorem is based on the assumption of a Gaussian noise (no multipath) environment, while the distribution of the received signal in the tunnel beyond the corner is closer to Rayleigh (high multipath). To account for additional reduction in channel capacity due to the multipath in the tunnel, the Shannon model can be modified using techniques described in, for example, [23, 24].

The Shannon capacity theorem is given by

$$C = B \log_2 (1 + S/N), \quad (9.3)$$

where  $C$  is the channel capacity in b/s,  $B$  is the channel bandwidth in hertz,  $S$  is the received signal power in watts, and  $N$  is the measured noise power in watts. The capacity represented by this equation is an upper limit. In reality, this capacity is difficult to attain with real hardware, and actual capacity of an uncoded signal can be closer to 50 % of the Shannon limit in a Gaussian noise environment. As mentioned above, since the tunnel environment is a high-multipath Rayleigh environment, the capacity may be reduced much lower than this, easily to 25% or less of the Shannon limit when the received signal is weak.

Because our robot used an analog video signal, Shannon's limit cannot be applied directly to estimate the channel capacity. However, the robot's control link was based on an IEEE 802.11b standard for digital transmission. The modulation bandwidth for an 802.11b transmission is 20 MHz. Figure 9.14 shows the Shannon channel capacity from Equation (9.3) for a system having a 20 MHz modulation bandwidth, a 2.44 GHz carrier frequency (the actual carrier frequency was somewhere between 2.412 and 2.462 GHz), 500 mW output power, and omnidirectional antennas (0 dBi gain). As before, we assume that the corner introduced 40 dB of attenuation. Figure 9.14(a) shows the Shannon capacity estimate along a 200 m path in the tunnel, with a right-angle turn at 100 m, and Fig. 9.14(b) is a close-up of the last 100 m only.

In an 802.11b system, the transmitted data rate reduces dynamically as the channel degrades, with a lower limit of 1 Mb/s when the received signal is weak or a great deal of interference exists. We see that at 160 m, where Table 9.2 shows that our robot started experiencing intermittent control, the data rate is on the order of 1 Mb/s if approximately 15% of the Shannon capacity is transmitted. We used formulas from [24] to find the additional reduction in capacity due to Rayleigh fading associated with the non-line-of-sight condition. This corresponds to a carrier-to-noise ratio of around  $-5$  dB, which is close to the excess link margin of  $-5.8$  dB at 160 m computed for this case. Note that the range the robot can travel can be

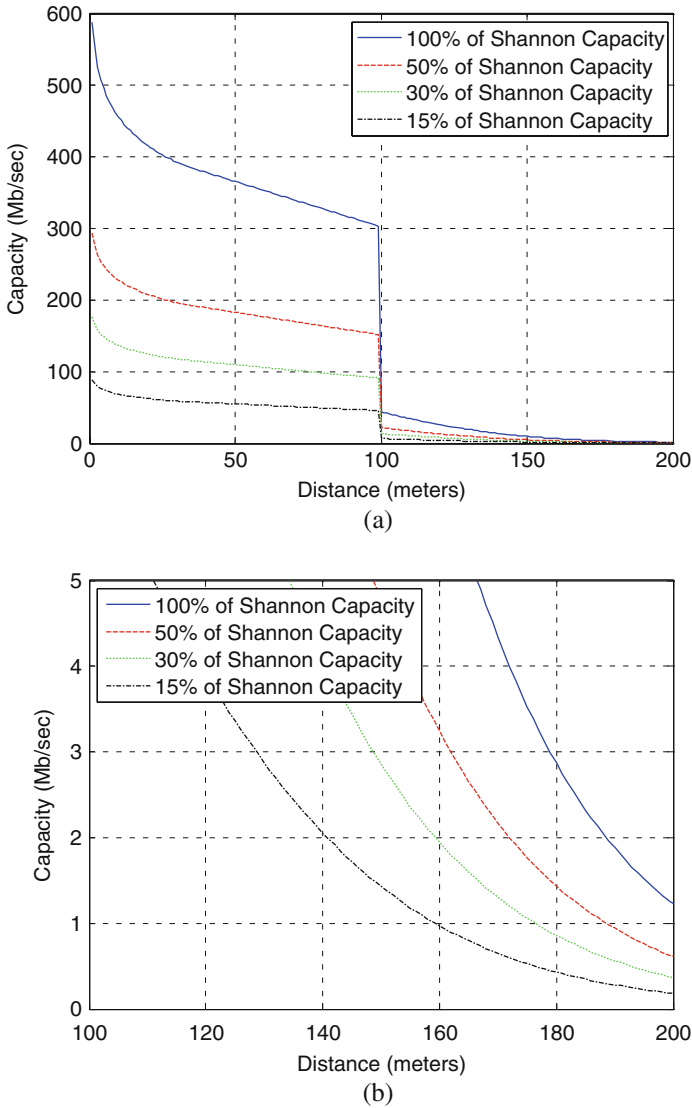


**Fig. 9.14** Channel capacity predicted by the Shannon theorem for a carrier frequency of 2.4 GHz and a modulation bandwidth of 20 MHz. At 160 m, where we experienced intermittent video, 15% of the Shannon limit is  $\sim 1$  Mb/s, which is the minimum data rate specified for an 802.11b signal before it fails

extended by using coding, signal processing techniques that include error correction. However, there is a limit to how far such signal processing can extend the range.

The above discussion presents a framework that may help the end user understand how to establish a bound for predictive planning. In practice there may be

many additional levels of performance evaluation that need to be carried out. Here we have provided illustrative examples that examine the effect of the propagation environment on the received-signal level (Section 9.4.1) and how the propagation environment impacts the transmission of a modulated signal, as discussed here.

## 9.5 Evaluating the Performance of a Robot in a Representative Tunnel Environment

In the previous two sections, we have conducted steps (1)–(4) in the performance evaluation procedure outlined in Section 9.2, and repeated here for convenience:

1. Develop an understanding of how signal impairments impact the performance of a specific wireless device or class of wireless devices.
2. Develop performance metrics that can be used to quantify this impact on performance.
3. Conduct measurements and/or simulations to determine the type and level of signal impairments to be expected in a given propagation environment.
4. Develop a model or gather sufficient measurement data in order to predict device performance in the presence of representative impairments.
5. Evaluate device performance when subjected to representative impairments by determining whether the signal impairments cause the device to exceed specified values of performance metrics. This can be done either through measurement verification or, at least for preliminary verification, with the models developed in step 4.

For step (1), we used prior knowledge of how signal impairments impact the performance of typical wireless devices to anticipate that reduced signal level and multipath would be the two key impairments for the US&R robot wireless link in a tunnel environment. For step (2), performance metrics for the control channel were identified as “go/no-go” operation of the robot. Performance metrics for the video link are still being developed, as discussed in Section 9.2 and [6, 7]. Thus, our performance evaluation consists of determining whether a robot will operate with certain parameters at various line-of-sight and non-line-of-sight ranges in the tunnel environment.

Step (3) was illustrated in Section 9.3, where we described measurements that enabled determination of the type and level of signal impairments in the tunnel environment. We saw that the received signal level was impacted by both standard free-space path loss signal attenuation and also by a lossy waveguide effect that significantly reduced received signal levels at the lower frequencies. Multipath was clearly seen in the form of peaks and nulls in the received signal across frequency. When a line-of-sight condition existed, structured deep nulls and peaks of the received signal across frequency could be seen as the direct-path signal and one or more strong reflected signals added destructively or constructively. In a non-line-of-sight

condition, the peaks and nulls took on a more random appearance. At the higher frequencies, the received signal level at times increased above the value that would be received in a free-space condition. This effect was again due to the waveguiding properties of the tunnel.

Step (4) was carried out in Section 9.4, where we used parameters of the specific tunnel environment in which we conducted our tests to predict the performance of the robot, both in terms of received signal power and in terms of channel capacity. The model results were verified by measurements of robot performance in the tunnel where the signal impairments were measured. The agreement between the model predictions and the robot measurements gave us confidence that the model could be used to predict robot performance in other tunnels; for example, those that are more representative of a typical emergency response scenario. This leads us to Step (5), where we try to determine whether the signal impairments in a representative environment would cause the robot to fail.

To predict and evaluate robot performance in a more representative tunnel, we used the model of Section 9.4.1 for a smooth-walled tunnel having dimensions of  $6 \times 4.5$  m, similar to those of a subway tunnel. The simulation, first presented in [21], was based on a scenario in which a subway train proceeds through a 1,500 m (approximately 5,000 ft) under-river tunnel, passing through a 200 m straight portion, through a large radius curve for the next 200 m, and then along a straight section. The subway train undergoes a major explosion when it is one-third of the way from the destination station in the direction of travel. The subway train stops at this location due to the explosion and a robot is deployed to search for victims (Fig. 9.15).

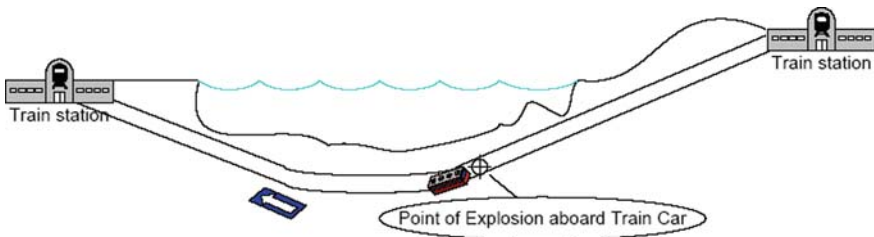


**Fig. 9.15** Representative tunnel environment consisting of a 1500 m smooth-walled underground tunnel with a large-radius curve. An environment such as this could be specified for the development of test methods to evaluate the performance of robots for US&R applications (drawing not to scale)

We demonstrate a method to predict and evaluate the received-signal level for a robot deployed in this environment using two models, one for the straight sections of the tunnel and one for the curvature in the tunnel. In Section 9.4, we verified the use of the model for the straight section. This model was also verified for use in a large roadway tunnel in [11]. Thus, we have a high degree of confidence that this model will allow us to evaluate the use of the robot in a subway tunnel. The model for the tunnel curvature was first presented in [21]. Because the curvature is

around a large-radius bend, the 90° turn from our measurements cannot be used. The model of [21], used here, is based on a physical representation of the tunnel, but to verify its performance, measurements or additional simulations would need to be conducted. As a result, the example presented in this section illustrates the method for predicting and evaluating robot performance, but additional work needs to be done before these results are used in practice.

Figure 9.16 shows the predicted path gain for each of the responder frequencies of interest using the path-loss model discussed in Section 9.4.1 combined with the model for the tunnel curvature from [21]. We plot only the first 1,000 m for clarity, where 0 m corresponds to the departure station. The propagation characteristics in each of the three tunnel sections (line-of-sight, curved, and non-line-of-sight) introduce different types and levels of signal impairments into the received signal. In reality, additional loss may be anticipated in some tunnels due to dampness of the walls and additional roughness from the track-bed and conduits, which will tend to absorb energy and increase path loss.

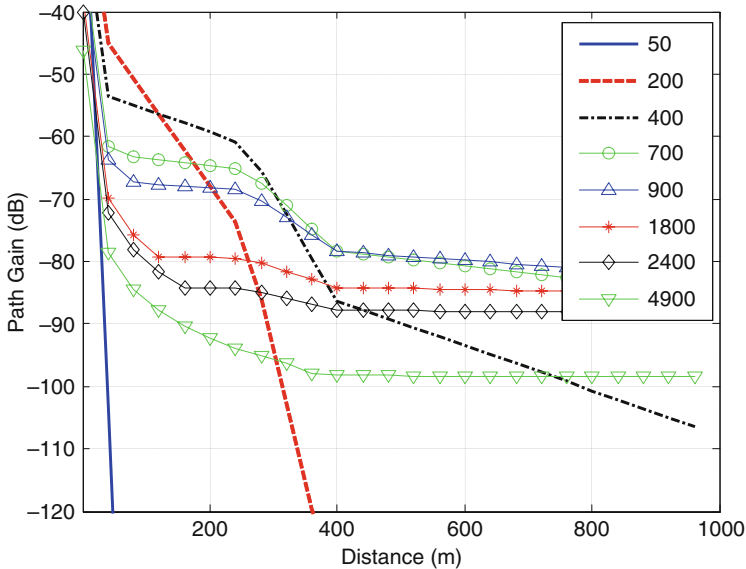


**Fig. 9.16** Path gain calculated for the 6 m × 4.5 m subway tunnel shown in Fig. 9.15 for eight different frequencies (in MHz). Three distinct propagation regions can be identified: Line-of-sight (less than 200 m), large-radius curve (200–400 m), and a straight, non-line-of-sight section (greater than 400 m) [15]

For short distances into the tunnel, where a line-of-sight condition exists, the lowest loss is seen between the 200 and 900 MHz frequencies. These results agree with the generalized trend that was seen in [11]; in that the frequencies in the middle range tend to provide the lowest path loss for shorter distances into tunnels of this size.

In the curved section of the tunnel, the loss tends to increase as the frequency decreases. From Fig. 9.16 we see that the 400 MHz signal decreases significantly in the large-radius bend. The rate of loss would increase in bends having a smaller radius of curvature.

For distances farther into the tunnel, beyond the curve, the model shows little difference in average signal loss between the frequencies of 700 MHz and 2.4 GHz. However, note that once the robot is in a non-line-of-sight condition, based on our observations in Fig. 9.9(b) and [5], we would expect the rapid variation in signal amplitude due to multipath is greater at higher frequencies. Dudley et al. [11] concluded that in both straight and curved tunnels there is little benefit in using increasing frequencies beyond a point where the attenuation (or ELM) flattens as frequencies increase. This will depend to some degree on the dimensions of the tunnel, but for the purpose of subway-sized tunnels, there is little to be gained in operating above 1.5 GHz.

This scenario illustrates a representative tunnel environment for US&R robot deployment that could be used for evaluating the performance of the wireless link for robots used in stand-off, tunnel-based applications where the operator is located in a non-line-of-sight condition from the incident. The scenario contains a number of key environmental elements that are specific to tunnels, including a line-of-sight portion where waveguiding effects occur, a curved section where frequency-dependent loss occurs, and a non-line-of-sight section where significant multipath occurs. The received signal level predicted by this model is only one component of a comprehensive performance evaluation; however, it serves to illustrate the performance evaluation method effectively.

A standardized test method, such as the non-line-of-sight test method described in Section 9.2 that captures the key signal impairments presented by this scenario, could be developed. The performance of robots for use in US&R applications could then be evaluated under these conditions. This would be a natural evolution for the ASTM standard described above and would complete Step (5) in the performance evaluation procedure.

## 9.6 Conclusion

We have presented a framework for evaluating the performance of the wireless link used in urban search and rescue robots, using a subterranean tunnel as an example of a representative responder environment. The evaluation method is based on extraction of the type and level of key signal impairments in a tunnel environment through measurement of the propagation characteristics of the tunnel. A model is then developed so that robot performance can be predicted in a representative class of (tunnel) environments. Using the model, representative values of key signal impairments can be replicated in a test environment to evaluate the expected performance of robots in a class of propagation environments; that is, in other tunnels. Real-time performance evaluation can also enable a robot to compensate for degradation of channel

characteristics by, for example, automatically deploying repeaters or changing the digital modulation format to one that is optimized for a given environment.

Results showed effects of waveguide-below-cutoff propagation and wall attenuation in the tunnels we measured, which agree with previously published results. We saw frequency-dependent peaks and nulls in the channel due to strong multipath reflections and attenuation in the tunnel. In non-line-of-sight conditions, we saw classic small-scale fading, manifested in noise-like multipath effects.

We implemented models of radio propagation and channel capacity within the tunnel environment and discussed how the models could be verified by measuring the performance of a robot within the tunnel and comparing the measured and modeled results. Note that more comprehensive performance evaluation procedures may also be carried out, where detailed models of the so-called physical layer would be constructed, including the effects of modulation, coding, equalization, power control, rate adaptation, etc. The goal of the work presented here was to illustrate some simple methods to predict and/or evaluate the expected over-the-air performance of a robot in a tunnel for other, more representative tunnel environments. An example of this was presented for a subway tunnel containing a large-radius curve. Such an example could provide the basis for a standardized test method to evaluate the line-of-sight and non-line-of-sight range performance of robots in tunnel environments for US&R applications.

**Acknowledgments** We gratefully acknowledge the contributions of the following: Chriss Grosvenor of the Electromagnetics Division of NIST and Dr. Robert Johnk of the Institute for Telecommunications Science (formerly of NIST) for assistance with the measured data; Dr. Bert Coursey, Director of the DHS Office of Standards and Elena Messina and Adam Jacoff of NIST's Manufacturing Engineering Laboratory for funding and supporting this work; Dr. Alex Bordetsky of the Naval Postgraduate School for facilitating the measurements during recent interagency marine interdiction operation system tests; Bill Dunlop, Steve MacLaren, and Dave Benzel of Lawrence Livermore National Laboratory for logistical and technical support; Roger Epperson, Park Supervisor and Gary Righettini, Mine Manager of the East Bay Regional Park District and the Black Diamond Mines Regional Preserve, for allowing us to conduct measurements; Frederick M. Remley for details on the NTSC video standard.

## References

1. E.Messina, "Performance Standards for Urban Search and Rescue Robots," *ASTM Standardization News*, August 2006. [http://www.astm.org/cgi-bin/SoftCart.exe/SNEWS/AUGUST\\_2006/messina\\_aug06.html](http://www.astm.org/cgi-bin/SoftCart.exe/SNEWS/AUGUST_2006/messina_aug06.html).
2. National Institute of Standards and Technology, *Statement of Requirements for Urban Search and Rescue Robot Performance Standards-Preliminary Report*. [http://www.isd.mel.nist.gov/US&R\\_Robot\\_Standards/Requirements%20Report%20\(prelim\).pdf](http://www.isd.mel.nist.gov/US&R_Robot_Standards/Requirements%20Report%20(prelim).pdf).
3. K.A. Remley, G. Koepke, E. Messina, A. Jacoff, and G. Hough, "Standards development for wireless communications for urban search and rescue robots," *Proceedings of the International Symposium on Advanced Radio Technol.*, pp. 66–70, Boulder, CO, Feb. 2007.
4. C.L. Holloway, W.F. Young, G. Koepke, K.A. Remley, D. Camell, and Y. Becquet, "Attenuation of Radio Wave Signals Coupled Into Twelve Large Building Structures," *National Institute of Standards and Technology Note 1545*, Apr. 2008.
5. K.A. Remley, G. Koepke, C.L. Holloway, C. Grosvenor, D. Camell, J. Ladbury, D. Novotny, W.F. Young, G. Hough, M.D. McKinley, Y. Becquet, and J. Korsnes, "Measurements

- to support broadband modulated-signal radio transmissions for the public-safety sector,” *National Institute of Standards and Technology Note 1546*, Apr. 2008.
6. M.H. Pinson, S. Wolf, and R.B. Stafford, “Video performance requirements for tactical video applications,” *Proceedings of IEEE Conference on Homeland Security Applications*, 2007, pp. 85–90.
  7. C. Ford and A. Webster, “Introduction to Objective Multimedia Quality Assessment Models,” *Proceedings of the International Symposium on Advanced Radio Technology*, Boulder, CO, March 7–9, 2006, pp. 8–15.
  8. [http://www.3gpp.org/ftp/Specs/latest/Rel-7/25\\_series/](http://www.3gpp.org/ftp/Specs/latest/Rel-7/25_series/). See 3GPP TS 25.101, Annex B.
  9. A.G. Emslie, R.L. Lagace, and P.F. Strong, “Theory of the propagation of UHF radio waves in coal mine tunnels,” *IEEE Transactions on Antennas and Propagation*, vol. 23, no. 2, Mar. 1975, pp. 192–205.
  10. M. Rak and P. Pechac, “UHF propagation in caves and subterranean galleries,” *IEEE Transactions on Antennas and Propagation*, vol. 55, no. 4, April 2007, pp. 1134–1138.
  11. D.G. Dudley, M. Lienard, S.F. Mahmoud, and P. Degauque, “Wireless propagation in tunnels,” *IEEE Antennas and Propagation Magazine*, vol. 49, no. 2, April 2007, pp. 11–26.
  12. C. Nerguizian, C.L. Despina, S. Alles, and M. Djadel, “Radio-channel characterization of an underground mine at 2.4 GHz,” *IEEE Transactions on Wireless Communication*, vol. 4, no. 5, Sept. 2005, pp. 2441–2453.
  13. M. Ndoh, G.Y. Delisle, and R. Le, “An approach to propagation prediction in a complex mine environment,” *Proceedings of the 2003 International Conference on Applied Electromagnetics and Communication (ICECom)*, Oct. 2003, pp. 237–240.
  14. M. Ndoh, and G.Y. Delisle, “Underground mines wireless propagation modeling,” *Proceedings of the 2004 IEEE Vehicular and Technology Conference*, Sept., 2004, pp. 3584–3588.
  15. D. Didascalou, J. Maurer, and W. Wiesbeck, “Subway tunnel guided electromagnetic wave propagation at mobile communications frequencies,” *IEEE Transactions on Antennas and Propagation*, vol. 49, no. 11, Nov. 2001, pp. 1590–1596.
  16. C.E. Shannon, “Communication in the presence of noise,” *Proceedings of IRE*, vol. 37, no. 1, Jan. 1949, pp. 10–21.
  17. M. Rütshlin, K.A. Remley, R.T. Johnk, D.F. Williams, G. Koepke, C. Holloway, A. MacFarlane, and M. Worrell, “Measurement of weak signals using a communications receiver system,” *Proceedings of the International Symposium on Advanced Radio Technology*, Boulder, CO, March 2005, pp. 199–204.
  18. P. Delogne, *Leaky Feeders and Subsurface Radio Communications*, IEEE Press, New Jersey, 1982.
  19. B. Davis, C. Grosvenor, R.T. Johnk, D. Novotny, J. Baker-Jarvis, and M. Janezic, “Complex permittivity of planar building materials measured with an ultra-wideband free-field antenna measurement system,” *NIST Journal of Research*, vol. 112, no. 1, Jan.–Feb., 2007, pp. 67–73.
  20. K.A. Remley, G. Koepke, C. Grosvenor, R.T. Johnk, J. Ladbury, D. Camell, and J. Coder, “NIST tests of the wireless environment in automobile manufacturing facilities,” *National Institute of Standards and Technology Note 1550*, Oct. 2008.
  21. G. Hough, “Wireless robotic communications in urban environments: issues for the fire service,” Thesis, Naval Postgraduate School, March 2008. [http://theses.nps.navy.mil/08Mar\\_Hough.pdf](http://theses.nps.navy.mil/08Mar_Hough.pdf).
  22. J. Lee and H. Bertoni, “Coupling at cross, T, and L junctions in tunnels and urban street canyons,” *IEEE Transactions on Antennas and Propagation*, vol. 51, no. 5, May 2003, pp. 926–935.
  23. A. Goldsmith, *Wireless Communications*, Cambridge University Press, Cambridge, MA, 2005.
  24. W.C.Y. Lee, “Estimate of channel capacity in Rayleigh fading environment,” *IEEE Transactions on Vehicular Technology*, vol. 39, no. 3, Aug. 1990, pp. 187–189.